

Generalizing the Dubins and Reeds-Shepp cars: fastest paths for bounded-velocity mobile robots

Andrei A. Furtuna, Devin J. Balkcom
Hamidreza Chitsaz, Paritosh Kavathekar

Abstract—What is the shortest or fastest path a mobile robot can follow between two configurations in the unobstructed plane? The answer to this fundamental question is only known analytically for a few planar mobile robots: the Dubins and Reeds-Shepp steered cars, the differential drive, and a particular omnidirectional robot. This paper explores the optimal trajectories for a general parameterized model of a mobile robot that includes each previously-studied vehicle as a special case. The model also allows characterization of the optimal trajectories for several other mobile robot designs for which the optimal trajectories have not been previously explored.

The paper applies Pontryagin’s Maximum Principle to the generalized robot to find necessary conditions that optimal trajectories must satisfy, and gives geometric interpretations of the conditions. We also present an algorithm that generates and classifies all optimal trajectories for a given design.

I. INTRODUCTION

There may be an infinite set of paths that connect a start and goal configuration for a mobile robot. Some of the paths will be faster or shorter than the others. This paper presents some geometric conditions on the fastest paths for simple kinematic models of mobile robots in the unobstructed plane.

The optimal paths are only known analytically for four ground vehicles: Dubins and Reeds-Shepp steered cars, the differential-drive, and the symmetric three-wheeled omnidirectional vehicle. This paper addresses the following question: can the optimal trajectories for these and similar but unstudied systems be explained by a single more-general model?

Understanding optimality is both basic and useful. A forklift robot operating in a constrained factory environment should have a different design than a race car. Knowledge of the analytical optimal trajectories may allow alternate mechanical designs to be considered rapidly, independently of the particular planning or control system implemented on the robot.

Figure 1 shows the model. There are three *omniwheels*, like those used to build both omnidirectional robots and certain types of conveyer belts. Omniwheels slip sideways freely, but like standard wheels, slip only minimally in the direction they are facing.

Different placements of the wheels lead to different kinematics for the system. Figure 2 shows how both a differential-drive and the Dubins and Reeds-Shepp steered cars can be built using omniwheels. For example, a differential-drive can be built by placing omniwheels at the same place on the robot as rubber wheels would be placed; these are the wheels labeled by the controls u_1 and u_2 in

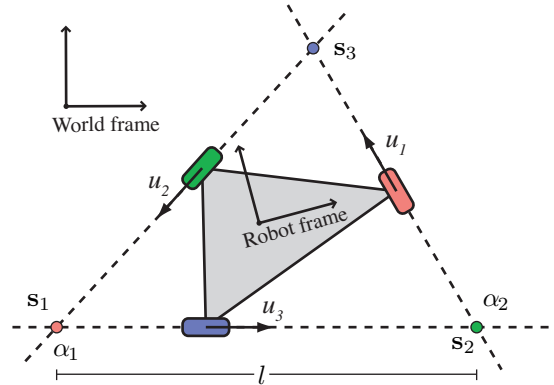


Fig. 1: A ‘generalized’ wheeled vehicle. With appropriate constraints on the controls, this vehicle can simulate any bounded-velocity rigid body in the plane.

figure 2. However, since these wheels are omniwheels, these two wheels are not enough – the robot can slip sideways freely, and its motion is not determined completely by the controls. We therefore place a third wheel on the line between the first two wheels, perpendicular to the first two wheels, and set the corresponding control u_3 to be zero.

The state of the robot is its position and orientation in the plane, given by the coordinates (x, y, θ) . There are three wheels; the speeds of the wheels in the facing direction, (u_1, u_2, u_3) , determine the velocity and angular velocity of the robot.

The placement of the wheels on the robot and the bounds on the wheel velocities both affect the optimal trajectories. Some of the results in this paper are applicable regardless of the bounds on the controls. The main result of this type is that for every optimal trajectory there is a line in the plane (the *control line*). The location of the control line depends on the the start and goal configurations, on the system equations, and on the control bounds, but is fixed for the duration of the trajectory. At each time along the trajectory, the generalized velocity of the robot must maximize the dot product between $(\dot{x}, \dot{y}, \dot{\theta})$ and (v_x, v_y, η) , where (v_x, v_y) is a unit vector parallel to the line, and η is the distance of the reference point on the robot from the line.

Most of the results of the paper deal with the special case where the bounds on the speeds of the wheels are independent; *i.e.*, the only constraints are that $u_1 \in U_1, u_2 \in U_2, u_3 \in U_3$, where U_1, U_2 , and U_3 are sets with both minimum and maximum elements. The previously-studied systems all can be seen to fall into this class, so long as the

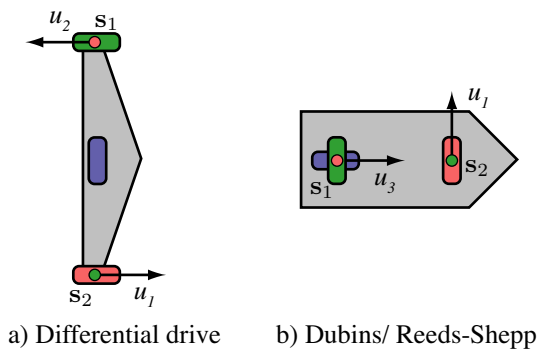


Fig. 2: Models of differential drives, Dubins cars, and Reeds-Shepp cars built using omniwheels.

omniwheels are placed in the right locations.

There are three main results about the time-optimal trajectories of the omniwheeled robot with independent controls.

- 1) Every optimal trajectory is composed of arcs of circles and straight lines.
- 2) There are three switching points attached to the robot, at the intersections of the lines through the wheels. If a switching point falls below the control line, the corresponding wheel spins at maximum speed in the forward direction; above the line, and the wheel spins at maximum speed in the reverse direction. If a switching point falls on the line, the robot may translate along the line.
- 3) We present a geometric algorithm that enumerates all optimal trajectory classes for a given vehicle design.

For a given start and goal, the location of the control line is hard to determine, but one point on the line can be determined within a (small) finite set of possible locations. Although we do not discuss the details in this paper, this reduces the problem of finding the optimal trajectory between a start and goal to a one-dimensional root-finding problem.

A. Background and related work

The structures of the optimal trajectories have been previously found for kinematic models of four vehicles: a steered car that can only go forwards (Dubins [3]), a car that can also go backwards (Reeds and Shepp [6]), the common differential-drive robot (Balkcom and Mason [2]) and the symmetric three-wheeled omnidirectional robot (Balkcom, Kavathekar and Mason [1]).

Reeds and Shepp's results were further refined by several authors. Sussmann and Tang [12] reduced the number of families of trajectories thought to be optimal by two, and Souères and Boissonnat [9], and Souères and Laumond [10] discovered the mapping from pairs of configurations to optimal trajectories.

All of these results were achieved by using bounded-velocity, kinematic models. Although ignoring accelerations is not completely satisfying, the optimal-control problem for dynamic models of ground vehicles appears to be very difficult; the differential equations describing the trajectories do not have recognizable analytical solutions, and in some

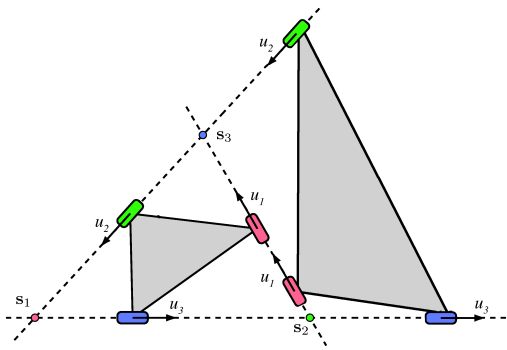


Fig. 3: Two robots sharing the same design class. Their wheel lines and switching points are identical.

cases, the optimal trajectories involve chattering, an infinite number of control switches in a finite time [11]. Tight bounds on the optimality of the derived solutions have proven difficult to determine, as has complete characterization of the geometric structure of trajectories, even though papers by Reister and Pin [7], and Renaud and Fourquet [8] present numerical and partial geometric results for steered cars, and Kalmár-Nagy *et al.* [4] present algorithms for numerically computing optimal trajectories for a bounded-acceleration model of the symmetric omnidirectional robot.

II. MODEL AND KINEMATICS

The robot is a rigid body, with state $q = (x, y, \theta)$, the location and orientation of a frame attached to the robot with respect to a fixed reference frame. Let $\hat{q} = (\hat{x}, \hat{y}, \hat{\theta})$ be the generalized velocity of the robot in its own frame of reference. The relationship between the generalized velocities in the two frames of reference is given by

$$\dot{q} = R(\theta)\hat{q}, \quad (1)$$

where

$$R(\theta) = \begin{bmatrix} \cos \theta & -\sin \theta & 0 \\ \sin \theta & \cos \theta & 0 \\ 0 & 0 & 1 \end{bmatrix}. \quad (2)$$

We define a bounded-velocity rigid body to be any rigid body in the unobstructed plane with $\hat{q} \in V$, where V is a set with boundary. In this paper we will only consider cases where V is invariant to changes in q .

Let u_i be the component of the velocity of the i th wheel in the controlled direction, as shown in figure 1. We place bounds on the controls: $u_i \in [l_i, h_i]$, for $l_i, h_i \in \mathbf{R}$ with $l_i < h_i$.

We would like to find a mapping from the controls u to the generalized velocity \dot{q} , and we expect that mapping to be linear:

$$\dot{q} = Bu. \quad (3)$$

The mechanism is parallel, so to find B , we will find the mapping from robot velocities to controls, and then invert that mapping.

Since translating one of the wheels along its wheel line will not change the mapping between controls and velocities,

the design of the robot can be given by any three numbers that describe the (possibly open) triangle formed by the intersections of the wheel lines, with vertices s_1 , s_2 , and s_3 (see figure 1). We call this triangle the *switching triangle*. All robots that share the same switching triangle are equivalent, forming a single design class (see figure 3). We choose to use a side length, l , and two angles, α_1 and α_2 , to describe the switching triangle, as shown in figure 1.

The plane velocity of a point at the intersection of two wheel lines depends only on the speeds of the two wheels that lie along those lines. It is therefore convenient to fix the robot frame to a vertex of the switching triangle, and align the x axis of the robot frame with one of its sides.

We collect all the terms dealing with the robot's design into a single matrix A , mapping between velocities and controls in the robot's frame. With this choice of reference frame,

$$A = \begin{bmatrix} \cos \alpha_2 & \sin \alpha_2 & l \sin \alpha_2 \\ \cos \alpha_1 & -\sin \alpha_1 & 0 \\ 1 & 0 & 0 \end{bmatrix}, \quad (4)$$

and

$$A^{-1} = \begin{bmatrix} 0 & 0 & 1 \\ 0 & -\csc \alpha_1 & \cot \alpha_1 \\ \frac{\csc \alpha_2}{l} & \frac{\csc \alpha_1}{l} & -\frac{\cot \alpha_1 + \cot \alpha_2}{l} \end{bmatrix}. \quad (5)$$

We will assume for the remainder of the paper that the placement of the wheels is such that the three lines through the wheels in the controlled directions are unique, not all parallel, and do not intersect at a single point. In this case, A is non-singular, B exists, and

$$\dot{q} = Bu = RA^{-1}u. \quad (6)$$

A. Centers of rotation

Theorem 1: The vehicle follows either an arc of a circle of a straight line over any interval during which the controls are constant.

Proof: Direct from integration of equation 6. ■

In the robot reference frame, the center of rotation O is located at

$$\begin{pmatrix} -\frac{\dot{y}}{\omega} \\ \frac{\dot{x}}{\omega} \end{pmatrix}. \quad (7)$$

III. THE MAXIMUM PRINCIPLE

This section uses Pontryagin's Maximum Principle [5] to derive necessary conditions for time-optimal trajectories. The Maximum Principle states that if the trajectory $q(t)$ with corresponding control $u(t)$ is time-optimal then the following conditions must hold:

- 1) There exists a non-trivial (not identically zero) *adjoint function*: an absolutely continuous \mathbf{R}^3 -valued function of time, $\lambda(t)$,

$$\lambda(t) = \begin{pmatrix} \lambda_1(t) \\ \lambda_2(t) \\ \lambda_3(t) \end{pmatrix},$$

defined by a differential equation, the *adjoint equation*, in the configuration and in time-derivatives of the configuration:

$$\dot{\lambda} = -\frac{\partial}{\partial q} \langle \lambda, \dot{q}(q, u) \rangle \quad \text{a.e.} \quad (8)$$

We call the inner product appearing in equation 8 the *Hamiltonian*:

$$H(\lambda, q, u) = \langle \lambda, \dot{q}(q, u) \rangle. \quad (9)$$

- 2) The control $u(t)$ minimizes the Hamiltonian:

$$H(\lambda(t), q(t), u(t)) = \min_{z \in U} H(\lambda(t), q(t), z) \quad \text{a.e.} \quad (10)$$

- 3) The Hamiltonian is constant and non-positive over the trajectory. We define λ_0 as the negative of the value of the Hamiltonian.

A. Application of the Maximum Principle to time-optimal bounded-velocity rigid bodies in the plane

Theorem 2: The adjoint function corresponding to the time-optimal trajectories of a rigid body in the unobstructed plane, with configuration $q = (x, y, \theta)$, is

$$\lambda = \begin{pmatrix} k_1 \\ k_2 \\ k_1 y - k_2 x + k_3 \end{pmatrix}, \quad (11)$$

regardless of the controls for the system, so long as the controls are invariant under $SO(2)$ action.

Proof: For any rigid body, the configuration space velocity of the body in the universal (fixed) coordinate frame is given by

$$\dot{q} = R\hat{q}. \quad (12)$$

The adjoint equation is

$$\dot{\lambda} = -\frac{\partial}{\partial q} \langle \lambda, \dot{q}(q, u) \rangle \quad (13)$$

$$= -\begin{pmatrix} 0 \\ 0 \\ \lambda^T \left(\frac{\partial}{\partial \theta} R \right) \hat{q} \end{pmatrix}. \quad (14)$$

By direct integration, $\lambda_1 = k_1$ and $\lambda_2 = k_2$. Substitute these values back into the definition for λ_3 :

$$\dot{\lambda}_3 = k_1(s\dot{x} + c\dot{y}) - k_2(c\dot{x} - s\dot{y}). \quad (15)$$

From equation 12,

$$\dot{x} = c\dot{x} - s\dot{y} \quad (16)$$

$$\dot{y} = s\dot{x} + c\dot{y}. \quad (17)$$

Substitute into equation 15,

$$\dot{\lambda}_3 = k_1\dot{y} - k_2\dot{x}, \quad (18)$$

and integrate:

$$\lambda_3 = k_1 y - k_2 x + k_3. \quad (19)$$

■

B. Geometric interpretation of the adjoint for time-optimal rigid bodies

For time-optimal motion of the body, there exists a line of force in the plane such that the velocity and angular velocity of the robot should be chosen to maximize the power done against the force at every instant, subject to the constraints on the controls of the robot. The location and orientation of this line of force depend on the initial and final configurations of the robot, but are fixed for any given trajectory.

We can write out the Hamiltonian for rigid bodies as a function of the state, the time derivative of the state, and three constants:

$$H = k_1\dot{x} + k_2\dot{y} + \dot{\theta}(k_1y - k_2x + k_3). \quad (20)$$

We will assume for the moment that $k_1^2 + k_2^2 > 0$. Since the Maximum Principle requires us to choose minimizing controls for the Hamiltonian, uniform positive scaling of the constants does not affect the choice of controls; without loss of generality we assume that $k_1^2 + k_2^2 = 1$.

Define the *control line* to be

$$\mathcal{L} = \{(a, b) \in \mathbf{R}^2 : k_1b - k_2a + k_3 = 0\},$$

The locus of points (a, b) that satisfy $k_1b - k_2a + k_3 = 0$ is a line. The term $(k_1\dot{x} + k_2\dot{y})$ in the Hamiltonian is the component of the velocity vector that lies along this line, and the term $k_1y - k_2x + k_3$ is the distance of the point (x, y) from this line.

If $k_1^2 + k_2^2 = 0$, the line can be considered to be ‘at infinity’, and the robot simply chooses controls to maximize or minimize angular velocity.

The state of the robot and the values of k_1 , k_2 , and k_3 determine the controls. Therefore, the problem of finding the optimal trajectory from start state q_0 to goal state q_1 optimally is reduced to finding values for k_1 , k_2 , and k_3 that take the robot to the goal optimally.

Computing the values of the constants directly (or equivalently, finding the location of the control line) for a given start and goal is difficult. First, however, we will consider the nature of trajectories assuming an arbitrary placement of the control line. In this case it is convenient to attach the world coordinate frame to the control line. In this case, the expression for the Hamiltonian simplifies to

$$H = \dot{x} + y\dot{\theta}. \quad (21)$$

C. Switching functions

Since there are independent bounds on the speeds of the wheels, the power the robot exerts against the virtual line of force can usually be maximized by driving the wheels at full speed either in the forwards or backwards direction.

Theorem 3: For any time-optimal trajectory, there exist constants k_1 , k_2 , and k_3 , with $k_1^2 + k_2^2 + k_3^2 \neq 0$, and functions φ_1 , φ_2 , and φ_3 defined by

$$(\varphi_1 \quad \varphi_2 \quad \varphi_3) = \lambda^T R_\theta A^{-1}. \quad (22)$$

such that the vehicle follows the control law

$$u_i(t) \in \begin{cases} \{h_i\} & \text{if } \varphi_i(t) < 0 \\ [l_i, h_i] & \text{if } \varphi_i(t) = 0 \\ \{l_i\} & \text{if } \varphi_i(t) > 0. \end{cases} \quad (23)$$

Furthermore, the quantity λ_0 defined by

$$\lambda_0 = -(\varphi_1 \quad \varphi_2 \quad \varphi_3) u \quad (24)$$

is constant along the trajectory.

Proof: We can rewrite the Hamiltonian

$$H = \lambda^T R_\theta A^{-1} u. \quad (25)$$

Application of the Maximum Principle completes the proof. ■

We call the functions φ_1 , φ_2 , and φ_3 *switching functions*, since the controls switch when these functions change sign. Explicitly, the switching functions may be written

$$\varphi_j = k_1(a_{3j}y + a_{1j} \cos \theta - a_{2j} \sin \theta) - k_2(a_{3j}x - a_{1j} \sin \theta - a_{2j} \cos \theta) + k_3 a_{3j}. \quad (26)$$

where a_{ij} is the (i, j) element of the design matrix A^{-1} .

D. Geometric interpretation

Theorem 4: There exist three ‘switching points’, \mathbf{s}_1 , \mathbf{s}_2 , and \mathbf{s}_3 , rigidly attached to the robot, such that the signed distance of \mathbf{s}_i from the control line \mathcal{L} is equal to the switching function φ_i , up to scaling by the constant a_{3i} . The switching points fall at the intersection of the wheel lines, but may be ‘at infinity’ if the lines do not intersect.

Proof: Take $a_{3i} \neq 0$. Assume the coordinates of the point \mathbf{s}_i in the robot frame are given by

$$\mathbf{s}_i = \begin{pmatrix} -\frac{a_{2i}}{a_{3i}} & \frac{a_{1i}}{a_{3i}} \end{pmatrix}. \quad (27)$$

In the world coordinate frame, the location of \mathbf{s}_i is given by

$${}^w \mathbf{s}_i = \begin{pmatrix} x \\ y \end{pmatrix} + R(\theta) \mathbf{s}_i. \quad (28)$$

Define

$$\eta(x, y) = k_1y - k_2x + k_3 \quad (29)$$

to be the signed, scaled distance of the point (x, y) from the line \mathcal{L} . Direct computation shows that

$$a_{3i} \eta({}^w \mathbf{s}_i) = \varphi_i. \quad (30)$$

To show that the switching points lie at the intersection of the wheel lines, without loss of generality we place the robot frame at one of the intersections, as described in section II. We then use the expression for A^{-1} given by equation 5 to compute the locations for the switching points \mathbf{s} in terms of α_1 , α_2 , and l .

If $a_{3i} = 0$, then switching point i is ‘at infinity’. To determine when the control corresponding to switching function φ_i switches, we consider the angle that the vector (a_{1i}, a_{2i}) makes with the control line; details are left to the reader. ■

Figure 4 shows the geometric interpretation of the optimal control law. The third switching point is above the control

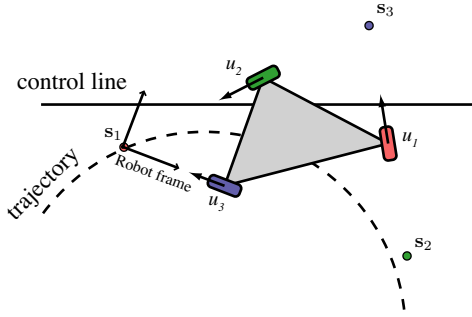


Fig. 4: The switching points' position relative to the control line determine the optimal control and the robot's trajectory.

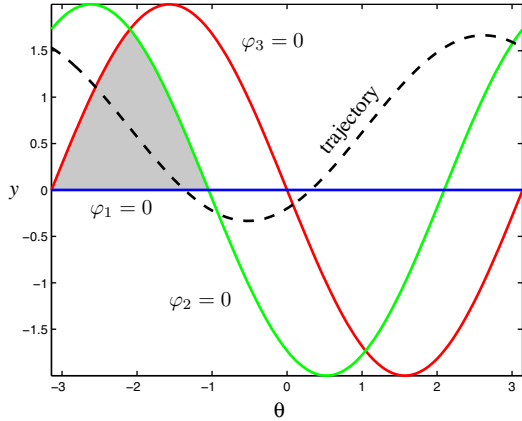


Fig. 5: A circle trajectory's image is a sinusoid in switching space. The robot will follow this trajectory as long as its configuration stays in the shaded region representing the control region appropriate for this circle segment.

line, causing its corresponding wheel to turn in reverse. The other two switching points are below, so u_1 and u_2 are maximal. This causes the robot to go on a circle. When this motion causes a switching point to cross the control line, its corresponding control will change, and so will the trajectory.

Notice that we can choose a convention for the signs on the controls so that a_{3i} is non-negative for all i . We therefore can drop the constant a_{3i} from the computation of the switching function, as long as we are careful about what happens when $a_{3i} = 0$.

If we align the world coordinate frame with the control line, the form of equation 28 is further simplified. Let (r_i, α_i) be the polar coordinates of switching point s_i in the robot frame. Then the switching function φ_i is

$$\varphi_i = y + r_i \sin(\theta + \alpha_i). \quad (31)$$

E. Optimal segments

The previous section gave a control law for optimal trajectories, as well as a geometric interpretation. We now turn to examine the implications of such a control law for the shape of optimal trajectories.

Theorem 5: If the trajectory of a bounded-velocity rigid body in the plane, with independent control constraints, is

singular on a non-null time interval, then the rigid body is translating in the control line's direction.

Proof: We will prove that θ is constant on such an interval. Assume that switching function φ_j is null at some moment. Then equation 31 indicates that y is a linear combination of $\sin \theta$ and $\cos \theta$, thus all three switching functions are linear combinations of these as well. Consider the time sub-interval before any other switching function becomes 0. Since the controls corresponding to the non-null switching functions are constant on this sub-interval, equation 24 indicates that the Hamiltonian becomes a linear combination of $\sin \theta$ and $\cos \theta$ as well:

$$H = k_1 \sin \theta + k_2 \cos \theta \quad (32)$$

where k_1 and k_2 are constants. Since the Hamiltonian cannot be zero, at least one of these constants is not null. Then let α be the direction of the (k_1, k_2) vector:

$$\frac{H}{\|(k_1, k_2)\|} = \sin(\theta + \alpha) \quad (33)$$

This equation has distinct roots, while θ is a continuous function of time. Therefore θ must be constant on the sub-interval considered. Furthermore, equation 31 implies that y is also constant, thus keeping all the switching functions constant on the sub-interval, so none of them can switch from a non-null to a null value. Therefore the sub-interval considered is identical to the whole singular interval. ■

Theorem 6: The time-optimal trajectories for any wheeled mobile robot in the unobstructed plane, with independent bounds on the speeds of the wheels, are composed only of arcs of circles and straight lines.

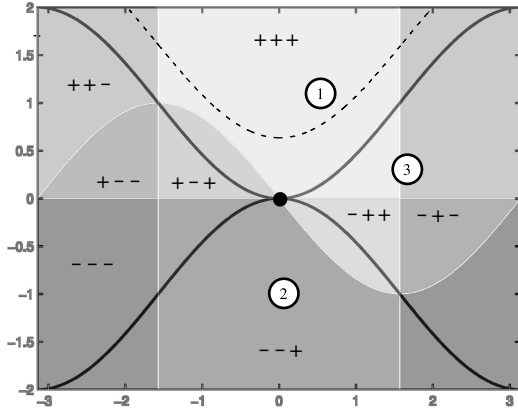
Proof: This follows directly from theorems 1 and 5 and equation 23. ■

IV. OPTIMAL TRAJECTORIES SUPERTYPES

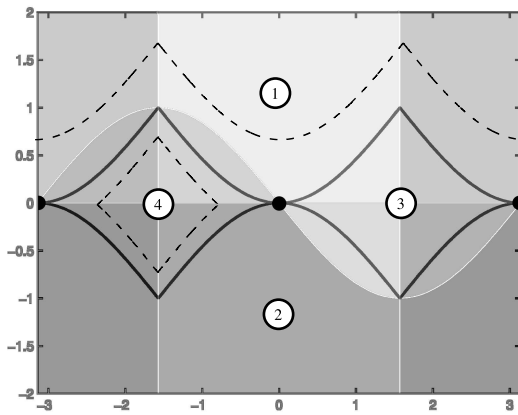
The previous section has identified the kinds of segments that optimal trajectories are composed of. How can these be fit together? We now proceed to a closer examination of the control switches, and the possible sequences in which they can occur. We will see that optimal trajectories can be grouped into well separated supertypes, according to these sequences, and we develop a method of enumerating these supertypes.

Although we cannot, at this point, determine the exact location of the control line, we can nevertheless enumerate all optimal trajectories for a given design by looking at all the possible configurations that the robot can have with respect to the control line. Only the robot's distance and orientation relative to the control line determine its optimal controls. Specifically, equation 31 indicates that, even though robot motion occurs in a three-dimensional configuration space, only two of these dimensions are relevant for applying the control law on optimal trajectories. It makes sense, therefore, to project these trajectories onto their y and θ dimensions, which we will call the *switching space*.

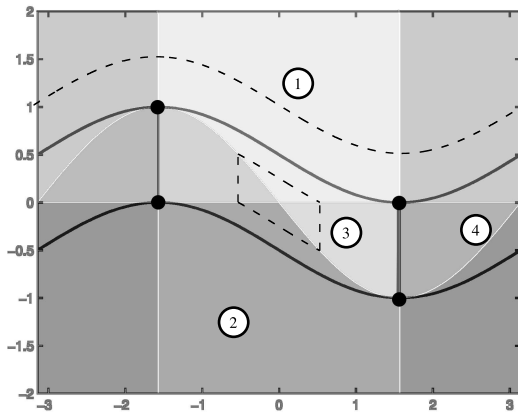
Given a robot configuration in switching space, we can determine the optimal controls by referring to the three



(a) The Dubins car.



(b) The Reeds-Shepp car.



(c) The differential drive.

Fig. 6: Separating the optimal trajectories for non-holonomic orthogonal vehicles in switching space. The shaded areas are control regions. The continuous lines are tangential trajectories, with the dots representing the points where translation along the control line is possible. The dotted lines show examples of non-tangential trajectories, with the numbers representing the non-tangential trajectory supertypes.

curves described by setting the switching functions to equal 0 (see equation 31).

Together, these sinusoidal curves divide switching space into 8 control regions, each characterized by its own set of extremal controls (see fig. 6(a) for an example). For example, the so-called $-++$ region is composed of all the points which are below the first switching curve, but above the other two. All robot configurations that fall into this region will share optimal controls that set u_1 to its maximum bound, and u_2 and u_3 to their minimum bounds.

Each optimal trajectory then appears as a continuous curve in switching space, a curve that changes its controls (and general appearance) each time it crosses a boundary between control regions. The crossings are usually instantaneous, with only singular trajectories being able to dwell on the boundaries for undetermined amounts of time.

As shown in theorem 6 above, optimal trajectories are composed of segments of lines and circles. Translation will show up in switching space as either a point (if it is parallel to the control line) or a vertical line. Rotation projects to a sinusoid. Each of these curves also needs to be intersected with the control region that makes it possible. An example is presented in figure 5, where the circle described by $+--$ controls is projected into switching space and intersected with the $+--$ control region.

Theorem 3 indicates that each optimal trajectory is characterized by its λ_0 quantity. Given this λ_0 , it is then possible to use the above method and identify all 8 optimal curve segments which correspond to it. By examining how they connect (through visual inspection, or a simple graph search), we can then determine the structure of all optimal trajectories corresponding to this λ_0 value. All these optimal segments, taken together, compose a λ_0 level curve.

Each λ_0 level curve contains a potentially infinite number of optimal trajectories, since it is possible to start and end anywhere on it, as long as travel proceeds continuously, with the possibility of periodicity as well; see figure 6(b) for two examples. We can distinguish the *optimal supertypes* appearing on a level curve by first separating the unconnected regions, and then picking start and end regions on each. For instance, suppose a level curve contains two disconnected boundaries. One goes through the $---$ and $--+$ control regions, while the other alternates between $+++$ and $+--$. This gives us two optimal supertypes, each of which contains many kinds of trajectory structures (such as partial segment $---$, full segment $---$, full segment $---$, partial segment $-+-$).

Small changes in the robot's orientation and distance to the control line will not change the control order (and thus the trajectory supertype), unless one of the circles that switching points follow around the rotation centers is tangent to the control line; we call trajectories where such a situation occurs *tangentials*. Drawing out the tangential level curves therefore separates the switching space into regions where all the level curves belong to the same supertype.

A particular category of tangentials are *singular trajectories*, where it is possible to keep translating along the control

line at the tangency point. In contrast to the region-bound supertypes, those containing singular trajectories are made up of parts of a single tangential level curve. Theorem 5, which indicates that translations have to be parallel to the control line, makes it possible to determine the points along a tangential curve (if any) at which singular segments of arbitrary length can occur.

Given the small number of possible circular optimal segments, the λ_0 values for the tangentials can be calculated for each (switching point, circle center) pair from equation 21, which becomes

$$\lambda_0 = d_{SP,IC} \omega_{IC} \quad (34)$$

where $d_{SP,IC}$ is the distance between the switching point and the circle center, while ω_{IC} is the angular velocity for the rotation around this center. Using the robot design and control bounds, these can be easily calculated from formula 7 and equation 5.

The process of finding the optimal trajectory supertypes can be automated. We have developed and implemented an algorithm which, given a robot design and its control bounds, produces a graph of all its corresponding tangential level curves, thus allowing us to visually determine the structure of all supertypes for this robot. While the space limitations constrain us to skip a detailed exposition of this algorithm, it follows the general method outlined above. For producing the optimal segments, the main difficulty lies in intersecting sinusoids in switching space. This is overcome by finding the bounds on these segments through working in configuration space, where the problem is the simpler one of intersecting the circles on which the switching points move during a rotation with the control line. Specifically, for each (switching point, circle center) pair we find the θ intervals that make it possible to obtain the control corresponding to that particular circle, then for each circle we intersect the three corresponding interval sets, an operation which results in determining the θ interval where this circle is possible for the given λ_0 .

The following section will show some examples of this algorithm's output.

V. SOME EXAMPLES

Three well studied vehicles are the Dubins and Reeds-Shepp cars and the differential drive. Figure 2 has shown how to model these with omnivheels, and also how to obtain their switching points by drawing out and intersecting the wheel lines. Since the "middle" wheel can be moved along its line (as discussed in II), these three vehicles share the same design class, and only differ in their control bounds. The common switching triangle is degenerate (two wheel lines being parallel), with two switching points falling on the wheels. The third switching point (only relevant for the Reeds-Shepp car) is "at infinity". It "crosses" the control line when the parallel wheel lines also become parallel with the control line.

The eight control regions determined by the switching curves are indicated as shadings in figure 6. This figure shows

the output of the algorithm described above, thus indicating all the optimal trajectory supertypes. For the Dubins car, we see that the tangential level curves divide switching space into three regions, each corresponding to a supertype. One is on top; the optimal trajectories are similar in shape to the region's boundary, can be periodic, and cross three control regions: $++-$, $+ - +$ and $+++$ respectively. Since only the u_1 control can switch in the Dubins car, this corresponds to a constantly right-turning trajectory, where u_1 is set to its lowest bound. The analysis of the bottom region is similar, and results in a constantly left-turning trajectory. The middle region (which wraps around in the cylindrical space) has level curves which are periodical, similar in shape to its boundary, and go in succession through all the control regions: $++-$, $+ - -$, $+ - +$, $- - +$, $- - -$, $- + -$, $- + -$, $+++$. This effectively results in a succession of left- and right-turns (*scrL r*, in Reeds and Shepp's notation), with maximum controls.

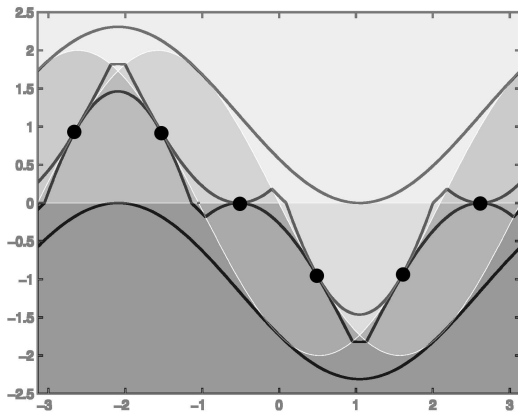
Given the vehicle's design, singular trajectories are only possible by setting u_1 to 0 at the point where y and θ are 0 as well. The tangential level curve indicated on the figure constitutes by itself a fourth, singular, supertype, containing, in addition to the left- and right-turns generated by the control regions which it passes through, line segments of arbitrary length at the (0, 0) point in the switching space. Optimal trajectories belonging to this supertype can therefore consist of any succession of maximum left- and right-turns and straight driving (e.g. *scrL s r*), with all the straight driving segments colinear.

Let us now move to a somewhat more complicated example, the Reeds-Shepp car (see figure 6(b)). The switching space is divided into 4 areas by the single tangential level curve. With u_2 fixed, the upper region corresponds to keeping u_1 minimized and alternating u_3 between its bounds. This results in a (forward-right, reverse-right) ($r^+ r^-$) supertype. Analogously, the lower region corresponds to a (forward-left, reverse-left) (*scrL⁺ scrL⁻*) supertype. The right middle area indicates the succession $+++$, $++-$, $-+-$, $-++$, corresponding to a (reverse-right, forward-right, forward-left, reverse-left) supertype, while the left middle area gives us (forward-left, forward-right, reverse-right, reverse-left).

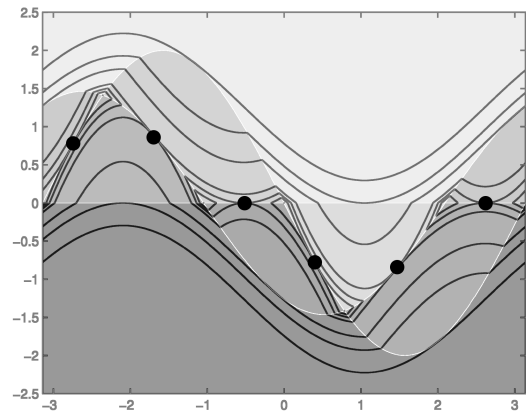
In addition to the 4 non-singular supertypes, there also exists one singular supertype, containing the tangential curve itself. The design of the robot makes possible translations along the control line at two points, (0, 0) and (π , 0) (identical to ($-\pi$, 0)). One example of such a singular trajectory is (forward-left, forward-straight, forward-left, reverse-left, reverse-straight, reverse-right).

The 5 optimal supertypes for the differential drive (fig. 6(c)) are left as an exercise to the reader.

For a non-orthogonal design, we first turn to robots such as Acroname's PPRK Brain Stem, which features three omnivheels placed symmetrically on the vertices of an equilateral triangle. The optimal trajectories for this robot have been determined recently (by Balkcom, Kavathekar and Mason in [1]). Its design being based on omnivheels, we extend and intersect the wheel lines to find that the switching



(a) The symmetric vehicle.



(b) An asymmetric vehicle.

Fig. 7: Switching space separation of separation of the optimal trajectories for omnidirectional non-degenerate vehicles.

triangle is a larger equilateral triangle, circumscribing the triangle formed by the wheels. Figure 7(a) presents the switching space of this robot, which features 1 singular and 10 non-singular subtypes, separated by 2 tangential level curves. The innermost 6 subtypes correspond to “shuffle” trajectories, the 2 between the level curves to “roll”, and the 2 outermost to “spin” respectively.

The complexity increases quickly if we allow the design to become asymmetric. Figure 7(b) presents the switching space for such an example, a hypothetical robot with a switching triangle that has $\frac{\pi}{3}$ and $\frac{\pi}{4}$ angles, which features 6 tangential level curves separating the switching space into 5 singular and 18 non-singular subtypes. Allowing asymmetric control bounds increases this complexity even further.

VI. OPEN PROBLEMS AND FUTURE WORK

While we are able to determine the optimal trajectory subtypes for any kinematic model of an omni-wheel-specified design, the problem of determining the optimal trajectory given specific start and end configurations remains open. We have made some progress towards determining the location of the control line; specifically we can find a small finite set of points which contains a point on this line, and we are able to determine its exact location for tangential trajectories. We are working towards determining its location in the general case.

REFERENCES

- [1] Devin J. Balkcom, Paritosh A. Kavathekar, and Matthew T. Mason. Time-optimal trajectories for an omni-directional vehicle. *International Journal of Robotics Research*, 25(10):985–999, 2006.
- [2] Devin J. Balkcom and Matthew T. Mason. Time optimal trajectories for differential drive vehicles. *International Journal of Robotics Research*, 21(3):199–217, 2002.
- [3] L. E. Dubins. On curves of minimal length with a constraint on average curvature and with prescribed initial and terminal positions and tangents. *American Journal of Mathematics*, 79:497–516, 1957.
- [4] Tamás Kalmár-Nagy, Raffaello D’Andrea, and Pritam Ganguly. Near-optimal dynamic trajectory generation and control of an omnidirectional vehicle. *Robotics and Autonomous Systems*, 46:47–64, 2004.

- [5] L. S. Pontryagin, V. G. Boltyanskii, R. V. Gamkrelidze, and E. F. Mishchenko. *The Mathematical Theory of Optimal Processes*. John Wiley, 1962.
- [6] J. A. Reeds and L. A. Shepp. Optimal paths for a car that goes both forwards and backwards. *Pacific Journal of Mathematics*, 145(2):367–393, 1990.
- [7] David B. Reister and Francois G. Pin. Time-optimal trajectories for mobile robots with two independently driven wheels. *International Journal of Robotics Research*, 13(1):38–54, February 1994.
- [8] Marc Renaud and Jean-Yves Fourquet. Minimum time motion of a mobile robot with two independent acceleration-driven wheels. In *Proceedings of the 1997 IEEE International Conference on Robotics and Automation*, pages 2608–2613, 1997.
- [9] P. Souères and J.-D. Boissonnat. Optimal trajectories for nonholonomic mobile robots. In J.-P. Laumond, editor, *Robot Motion Planning and Control*, pages 93–170. Springer, 1998.
- [10] Philippe Souères and Jean-Paul Laumond. Shortest paths synthesis for a car-like robot. *IEEE Transactions on Automatic Control*, 41(5):672–688, May 1996.
- [11] Héctor Sussmann. The Markov-Dubins problem with angular acceleration control. In *IEEE International Conference on Decision and Control*, pages 2639–2643, 1997.
- [12] Héctor Sussmann and Guoqing Tang. Shortest paths for the Reeds-Shepp car: a worked out example of the use of geometric techniques in nonlinear optimal control. SYCON 91-10, Department of Mathematics, Rutgers University, New Brunswick, NJ 08903, 1991.